Spectrochimica Acta Part A: Molecular and Biomolecular Spectroscopy 323 (2024) 124881

Contents lists available at ScienceDirect

Spectrochimica Acta Part A:
Molecular and Biomolecular Spectroscopy

journal homepage: www.journals.elsevier.com/spectrochimica-acta-part-a-molecular-and-biomolecular-spectroscopy

Silver nanoparticles from orange peel extract: Colorimetric detection of Pb^{2+} and Cd^{2+} ions with a chemometric approach

Marco Zannotti [a], Sara Piras [a], Lisa Rita Magnaghi [b,*], Raffaela Biesuz [b], Rita Giovannetti [a,*]

[a] School of Science and Technology, ChIP Research Center, Chemistry Division, University of Camerino, 62032 Camerino, Italy
[b] Department of Chemistry, University of Pavia, Viale Taramelli 12, 27100 Pavia, Italy

HIGHLIGHTS

- AgNPs@OPE nanoparticles was used as selective colorimetric sensor for Cd^{2+} and Pb^{2+}.
- The assay was based on the metal-induced aggregation of AgNPs@OPE.
- PLS allowed to quantify Cd^{2+} and Pb^{2+} in the concentration range 2.49—47.62 μM.
- PCA and LDA were used for the classification and distinction of Cd^{2+} and Pb^{2+}.

GRAPHICAL ABSTRACT

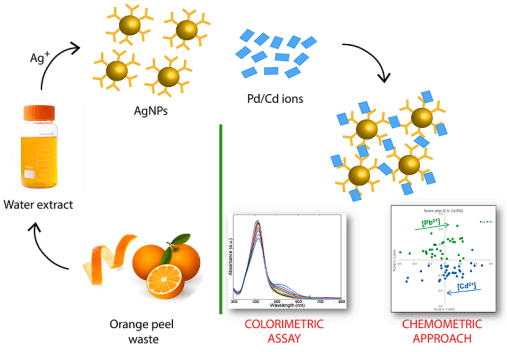

ABSTRACT

Green silver nanoparticles (AgNPs@OPE) were obtained by using orange (citrus sinensis) peel water extract (OPE) that acts as a reducing and capping agent. This procedure permits the valorisation of waste as orange peel, and lowers the environmental impact of the process, with respect to the conventional synthetic procedure. The OPE extract reduced Ag(I) to Ag(0) in alkaline conditions, and stabilised the produced nanoparticles as a capping agent. The AgNPs@OPE were deeply characterized by UV–Vis spectroscopy, FT-IR, SEM analysis and DLS analysis and successively used as colorimetric sensors for different metals in aqueous solution. The colourimetric assay showed that AgNPs@OPE were able to detect Pb^{2+} and Cd^{2+}, as demonstrated by the splits of surface plasmon resonance (SPR) band accompanied by the formation of a second new band; these spectral modification resulted in a colour change, from pristine nanoparticles' yellow to brown, due to the aggregation process. For the quantification of each of the two target cations, a calibration was performed by using the univariate linear regression, within the linearity ranges, exploiting the absorbance ratio between the main SPR band and the new band relative to the aggregate formation. Then a multivariate approach was followed to perform both Cd^{2+} and Pb^{2+} quantification by means of Partial Least Square regression (PLS) and target cations distinction by Linear Discriminant Analysis (LDA) applied on Principal Components Analysis (PCA) outputs, in both cases using the entire UV–Vis spectra (350–800 nm) as input data. Finally, the ability to quantify and distinguish between Cd^{2+} and Pb^{2+} was tested in tap water samples spiked with the two cations in order to confirm the application of the AgNPs@OPE as selective sensor in real samples.

* Corresponding authors.
E-mail addresses: lisarita.magnaghi@unipv.it (L. Rita Magnaghi), rita.giovannetti@unicam.it (R. Giovannetti).

https://doi.org/10.1016/j.saa.2024.124881
Received 16 April 2024; Received in revised form 8 July 2024; Accepted 22 July 2024
Available online 23 July 2024

1. Introduction

Heavy metals are among the most problematic water pollutants since they are dangerous for human health and the environment. They come from both anthropic sources (industries and agriculture) and natural sources (volcanic activity and soil erosion) [1]. Heavy metals tend to bioaccumulate in living organisms; they are toxic and carcinogenic for humans and can also affect aquatic organisms [2]. The most common heavy metals that can be find in wastewater are copper (Cu), cadmium (Cd), zinc (Zn), lead (Pb), mercury (Hg), arsenic (As), chromium (Cr), iron (Fe) and platinum (Pt) [2].

Lead is ranked as the second most hazardous pollutant after arsenic by the U.S. Environmental Protection Agency (USEPA) and the Agency for Toxic Substances and Disease Registry (ATSDR) [3]. Lead (II) ions can be released into the environment from batteries, cosmetics, pesticides, glass manufacturing and paint industry. Lead (II) is highly toxic and its concentration in drinking water and foods is limited by law.

Cadmium (II) ions are naturally present in the environment, but their concentration can increase to dangerous levels when released in great quantities from anthropogenic sources. Cadmium can be released in the environment from landfills or from its use in agriculture as phosphate fertilizer and from many industrial processes: it is in fact used as corrosive reagent, in colour pigments, in Ni-Cd batteries, as stabilizer in PVC products, etc [4]. Exposure to cadmium happens primarily from ingestion of contaminated food and water or through inhalation and cigarette smoke, and it can lead to serious health problems such as various types of cancer, osteoporosis, liver, and kidney disease.

The assessment and monitoring of lead and cadmium pollution is thus of paramount importance and many methods are currently employed, such as atomic absorption spectrometry, ion chromatography, and electrochemical techniques; however these techniques have the disadvantage of being time-consuming, expensive, and requiring trained professionals to be performed. Therefore, there is the urgent need of faster and easier methods which can detect the presence of heavy metal pollution in water: among all, colorimetric sensors based on metal nanoparticles are a promising technique for detecting heavy metal ions in water solutions.

Metal nanoparticles (MNPs) are a class of NPs made purely of metal (e.g., gold, silver, platinum, iron, etc.) or of metal-containing compounds, that can be modified by the means of various functional groups for a wide range of potential applications. In particular, noble metal nanoparticles such as silver nanoparticles (AgNPs) present unique optical properties [5,6] that depend on their size and shape, which can be easily tuned by changing the reaction parameters in the synthesis [7].

AgNPs show a characteristic localized surface plasmon resonance (SPR)resulting from the collective oscillation shown by the conduction electrons on the nanoparticle surface when excited by light at specific wavelengths. This oscillation, known as SPR, results in very strong scattering and absorption of light in the visible range: focusing on AgNPs with an average diameter of less than 100 nm this phenomenon occurs in the range 380 to 460 nm [8]. The frequency of SPR depends on nanoparticle composition, size, shape (spheres, rods, triangles, stars, cubes, etc.) and the surrounding environment [9,10].

The SPR and the absorption behaviour of nanoparticles can also change as a function of specific analytes and compounds added to the metal nanoparticles, causing a concomitant change in the colour of metal nanoparticle solutions. In the case of heavy metals, the cation added to the metal nanoparticles can induce particles aggregation by the interaction of the positive cations and the negative surface of the metal nanoparticles properly functionalised. In that case, the interparticle distance is reduced causing a shift in the SPR band with respect to the monodisperse nanoparticles [11,12]: the shift of the SPR band is accompanied by a colour change, that can be effectively used for colorimetric detection of a specific analyte in water solutions.

AgNPs can be synthesized by different procedures such as physical and chemical methods, the latter involving the reduction of metal salts. Chemical methods are the most used in the synthesis of metal nanoparticles because they present the advantage of being easily tuneable by modifying the strength and type of the reducing and capping agents [5]. Recently, the use of environment-friendly solvents, microorganism or plant extract has been suggested as a valuable alternative to traditional methods. These green syntheses reduce the usage of chemicals while keeping the pros of stabilizing agents [13,14].

The orange peel extract (OPE) contains phenolic substances such as flavonoids (FLs) that have an important role in the synthesis of metal nanoparticles, showing reducing character [15,16]. Different studies reported the synthesis of AgNPs using orange or citrus fruits peel extracts applied in photocatalysis, antimicrobial, antibacterial and antifungal activities, and in flavonoids determination [17–19].

In this study, an aqueous extract of orange (*Citrus sinensis*) peel was used as reducing and stabilizing/capping agent to produce silver nanoparticles (AgNPs@OPE). The synthesis of AgNP@OPE was optimized in terms of the used amount of the orange peel extrac t(OPE), and important, without the use of other stabilizing agent, such as PVP [20], or addition of helping amount of other reducing agent like $NaBH_4$ [18].

After the synthesis of AgNPs@OPE, the nanoparticles were characterized by UV–Vis, FT-IR, SEM and DLS analysis and employed as sensors colorimetric sensor for heavy metal cations in water, showing selectivity towards Cd^{2+} and Pb^{2+} ions.

The spectral modification registered upon addition of the two target metal ions were firstly exploited for quantification purposes by the means of univariate linear regression, within the linearity ranges defined per each analyte. This approach led to satisfactory results, especially in terms of sensitivity, but it unavoidably required some data manipulation to extract one single and meaningful concentration-dependent parameter from an extremely complex set of UV–Vis signals. To overcome this issue, a multivariate approach was later followed by submitting the entire UV–Vis spectra, registered upon Cd^{2+} or Pb^{2+} addition, to Partial Least Square regression (PLS) [21–23] and developing multivariate quantification models for each analyte.

Moreover, the ability of AgNPs@OPE to distinguish between Cd^{2+} or Pb^{2+}, regardless their concentration, was evaluated. It must be underlined that the previously described single metal ion quantification was actually feasible also by univariate approach, thus, multivariate tools have been exploited to avoid data manipulation. On the contrary, the distinction between the two metal ions could be performed only and exclusively by the means of specific multivariate tools due to the impact of metal ion concentration on AgNPs@OPE UV–Vis spectra, definitely stronger than the one exerted by metal ion type, and the high similarity of the signals in presence of Cd^{2+} or Pb^{2+}. To reduce data dimensionality and extract the desired information from the dataset, UV–Vis spectra were firstly submitted to Principal Component Analysis (PCA) [24] and, secondly, Linear Discriminant Analysis (LDA) was applied as classification tool, using the PCA scores as input variables [25].

Finally, both quantification and classification chemometric models were cross-validated following the proper approach described in the dedicated section and validated by predicting either metal ion concentration or type of new independent samples.

2. Materials and methods

2.1. Materials

Silver nitrate ($AgNO_3$), NaCl, $CaCl_2$, KCl, $NiCl_2$, $CoCl_2$, $ZnCl_2$, $CuCl_2$, $MnCl_2$, $FeCl_2$, $MgCl_2$, $CdCl_2$, $HgCl_2$, $PbCl_2$ were purchased from Sigma-Aldrich (St. Louis, MO, USA).

HCl and NaOH 2 M were acquire from Carlo Erba Reagents SAS (Chaussée du Vexin, Parc d'Affaires des Portes, Val de Reuil, France). All these chemicals were used as received without further purification. Fresh orange fruit (*Citrus sinensis*) was collected at the supermarket Eurospin, Camerino, Italia. All the solutions were prepared and diluted using ultrapure water (18.2 μS/cm) generated by Milli-Q® Advantage

A10, Merk.

2.2. Preparation of the water orange peel exctract (OPE)

The orange fruit was washed with deionized water, and the peel was separated and cut into small pieces. 30 g of peel was put into 100 mL of ultra-pure water and boiled for 10 min. The orange peel extract (OPE) was separated from the solid residue by a sift and then it was collected by filtration using a filter paper, followed by centrifugation at 6000 rpm. OPE was then stored in a refrigerator at 4 °C for subsequent use. The extract was then characterized by UV–Vis spectroscopy and the influence of pH was evaluated. The OPE was also lyophilized and the dried sample was analysed with IR spectroscopy.

2.3. Synthesis of AgNPs@OPE

Silver nanoparticles (AgNPs@OPE) was prepared in 20 mL vials, in a final volume of 10 mL of ultrapure water. Specifically, the AgNPs@OPE preparation was evaluated in neutral pH conditions with different amounts of water OPE extract (from 50 to 200 μL), and then the synthesis was repeated with the addition of different concentrations of NaOH from 1 to 5 × 10^{-3} M to evaluate the synthesis at different alkaline pH conditions. The shift from colourless to yellow in the color of the solution indicated the formation of AgNPs@OPE. The synthetic procedure was also monitored at different temperature conditions and stirring time.

The vials were sealed with a cap, protected from light with an aluminium foil, mixed with a magnetic stirrer at room temperature for 15 min and then heated at 60 °C for 1 h. The formation of the nanoparticles was monitored by UV–Vis measurements carried out by Agilent Cary 8454 Diode Array System spectrophotometer. The obtained nanoparticle suspension was dialyzed with a 3.5 kDa membrane (Spectra/Por Dialysis Membrane Standard RC Trial Kit bought from Spectrum Laboratories Inc., Rancho Dominguez, CA, USA) to remove the reagents in excess, and stored at 4 °C.

2.4. Characterization of AgNPs@OPE

The morphology of the AgNPs@OPE was analysed by SEM microscopy by using by using a field emission scanning electron microscope (FE-SEM, Sigma 300, Zeiss, Gina, Germany) at 3 kV and with energy-dispersive X-ray spectroscopy (EDX, Quantax, EDS, Bruker). Several drops of the silver nanoparticles were deposited on a Silicon foil that was placed on aluminium stubs by using self-adhesive carbon tabs; the liquid phase was then removed at 30 °C in a vacuum oven (Vismara, 65). The nanoparticles distribution was evaluated by using ImageJ software.

The functional groups of the surface ligands were investigated with Fourier-transform infrared spectroscopy (FT-IR), with Perkin-Elmer System 2000 FT-IR instrument (Waltham, MA, USA). For this purpose, the AgNPs@OPE dialyzed solution was previously lyophilized to obtain the nanoparticle pellet.

The size distribution and the Zeta-potential of the AgNPs@OPE nanoparticles were also explored with Dynamic light scattering measurements performed using a Malvern Zetasizer nano S device (Malvern Instruments, Worcestershire, UK) equipped with a back-scattered light detector operating at 173°.

2.5. AgNPs@OPE as sensor for heavy metals

Stock solutions of the following metal cations: Ca^{2+}, Cd^{2+}, Co^{2+}, Cu^{2+}, Fe^{2+}, Hg^{2+}, K^{+}, Mg^{2+}, Zn^{2+}, Na^{+}, Ni^{2+}, Mn^{2+} and Pb^{2+}, with a concentration of 1 mM, were prepared from the corresponding chloride salts and stabilized in acidic pH.

The selectivity of the colorimetric assay was tested adding the same concentration (about 80 μM) of different metal cations to AgNPs@OPE colloidal solution, diluted 1:1 in ultrapure water. For Cd^{2+} and Pb^{2+}, the UV–Vis spectral change with increasing concentration of the two metals ions (from 2.49 to 47.62 μM) to the AgNPs@OPE (1 mL AgNPs@OPE: 1 mL H_2O), was monitored. The calibration of the two cations was performed through univariate linear regression, within the linearity ranges, monitoring the absorbance ratio between the main SPR band and the new band relative to the aggregate formation. All the colloidal solutions were monitored after 15 min from the addition of the metal ions.

2.6. Chemometric approach to AgNPs@OPE UV–Vis spectra in presence of Cd^{2+} and Pb^{2+}

2.6.1. Training and test set

AgNPs@OPE UV–Vis spectra with increasing concentration of the two metal ions were employed as training set for all the multivariate techniques employed, resulting in a matrix made of 68 rows, i.e. samples, (2 replicate x 17 concentrations within 2.49 and 47.62 μM x 2 metal ions) and 450 columns, i.e. variables (absorbance in the range 350–800 nm, registered with an interval of 1 nm).

When required, an external test set was used to validate the model performances, both in terms of metal ions quantification and discrimination; the test set includes samples with either one single metal ion or both the analytes. As for the first case, 8 samples containing either Cd^{2+} or Pb^{2+}, in a concentration included in the range used for building the models (5.47, 17.20, 28.18 and 40.76 μM) were prepared; as for the samples containing both the metal ions, three values of cumulative metal ions concentration were selected (5.47, 28.18 and 40.76 μM) and, for each value, three samples were prepared with Cd/Pb ratios of 9:1, 1:1 and 1:9.

Finally, all the models developed were tested on fortified tap water samples to preliminarily assess the applicability of AgNPs@OPE in sensing Cd^{2+} and Pb^{2+} in real samples and their robustness towards matrix-related effects. The tap water used was fully characterized by ICP-MS (ICP-MS 7500cx series (Agilent Technologies, Santa Clara, CA, USA) and Ion-Chromatography (ICS-1000, Dionex-Thermo Fisher Scientific, Waltham, MA, USA.) The tap water was then fortified with either Cd^{2+} or Pb^{2+} at increasing concentrations (10.00, 15.00 and 30.00 μM); eventually the four following samples containing both metal ions were prepared: a) total metal content 35 μM with Cd-Pb ratio 6:1 and b) 1:6, c) total metal content 30 μM with Cd-Pb ratio 2:1 and d) 1:2 (Table S1).

2.6.2. Multivariate quantification by partial Least Square regression

The entire UV–Vis spectra of the samples in the training set, after column centering, were used to develop a multivariate quantification model per each metal ion (34 training samples per each model) using Partial Least Square regression [26]. The optimal number of latent variables (LV) is defined evaluating the Root Mean Square Errors in Cross-Validation (RMSECV) and in Prediction (RMSEP) for the models built using from 2 to 9 LV, computed as described in Eq. (1). All the calculations were performed using the open-source software CAT [27].

Eq. (1). RMSECV and RMSEP calculation

$$RMSECV = \sqrt{\frac{\sum \left(y_{CV\,pred} - y_{exp}\right)^2}{n^{\circ}\,training\,samples - 1}};\; RMSEP = \sqrt{\frac{\sum \left(y_{pred} - y_{exp}\right)^2}{n^{\circ}\,test\,samples}} \quad (1)$$

2.6.3. Multivariate discrimination by linear Discriminant analysis on principal components

The entire UV–Vis spectra of all the samples in the training set, after column centring, were used to develop a multivariate discrimination model able to distinguish between AgNPs@OPE solutions added with either Cd^{2+} or Pb^{2+}. Since most classification tools require training sets with more samples than variables, i.e. more rows than columns, but this condition was not verified in the training set (68 samples x 450 variables), Principal Component Analysis was first employed to reduce data dimensionality while keeping the information included in the original data and, secondly, PCA scores were used as input dataset to apply

Linear Discriminant Analysis (LDA). The developed model was first evaluated, analysing predictive performances by means of cross-validation; then, it was finally tested on the full test set, including both single metal ions and mixed samples.

2.6.4. Cross-validation approach

Cross-validation (CV) is actually the most widespread validation method in the field of multivariate data analysis. The general procedure is easily described here: the whole sample set is divided into a pre-defined number of subgroups, called cancellation groups and a "partial" model is computed as many times as the number of cancellation groups: each time, one of the cancellation groups is excluded from partial model building and used as a partial test set. At the end of the procedure, the average value of prediction abilities of all the subsets is calculated and provided as the CV final outcome [25]. Obviously, the number of cancellation groups and the criterium employed for their computation strongly influences not only the final CV results but mainly to which extent they do provide a realistic representation of model's predictive performances. In this case, in order to provide a realistic and robust prediction estimation, three cancellation groups were defined in which both the replicates for predetermined concentration levels were excluded, as described in detail in Table S2 in the case of single metal ion concentration (3 cancellation groups of 10/12 samples). This approach was chosen in order to avoid including one replicate of a given concentration in the partial training set and the other one in the cancellation group, thus leading to over-optimistic CV results. A similar approach was followed in the case of cations distinction, defining 3 cancellation groups of 22/24 samples by merging different single cation cancellation groups, in order to avoid removing from the partial training set the same concentration levels for both the metal ions.

3. Results and discussions

3.1. Characterization of water OPE extract

Fig. 1 displays the UV–Vis spectra of orange peel extract (OPE) in water at different pH conditions, showing the characteristic signals of phenolic compounds with changes in wavelength and in intensity as function of the pH [24]. The different colour change, yellow at acidic pH, orange at alkaline pH and almost transparent at neutral pH, could be attributed to the presence of flavonoids.

In the acidic and neutral conditions, the spectra show the presence of two main bands at about 280 nm, due to the benzoyl ring-related system, and at 320 nm, due to the localized transition within the cinnamoyl ring system. In addition, the spectra reveal absorption bands within the 200–234 nm range, which are characteristic of ester, carbonyl, carboxyl, and amine. functional groups [28].

The FT-IR profile of OPE extract, reported in Fig. 2, shows a broad peak at 3400 cm^{-1} attributable to the stretching vibration of –OH group of alcohols, phenols, flavonoids, –COOH groups and to the intra and inter-molecular bonding. The band at 2920 cm^{-1} is due to the –CH stretching of the aromatic compounds in the extract, the additional strong band at 1610 cm^{-1} corresponds to the typical stretching vibration of the C=C aromatic bond of the phenolic groups, and finally the bands at 1730, 1415 and 1013 can be associated with the C=O, –COOH and C-O functional groups, respectively [29]. The results confirm, according to literature, the presence of polyphenol and flavonoid compounds in the orange peel extract. These interesting compounds can be used as advantageous reducing agents for the formation of the green AgNPs@OPE. In particular, the flavonoids in the OPE solution show their maximum reductive ability in alkaline pH [20].

3.2. Synthesis of AgNPs@OPE

For the preparation of AgNPs@OPE, $AgNO_3$ is used as precursor and OPE extract as reducing and capping/stabilizing agent in different ratios and pH conditions. The obtained spectra (Fig. 3a) show that the SPR band at about 408 nm, characteristic of silver nanoparticles, presents the highest absorbance value by using 5×10^{-3} M of NaOH (pH=11.5). During the nanoparticle formation the solution turns from colourless to yellow, with a different colour shade depending on the quantity of NaOH employed in the reaction (Fig. 3 a,c). The influence of OPE extract is investigated by monitoring the SPR band of the obtained AgNPs@OPE in alkaline pH (11.5). The plot in the Fig. 3b depicts the UV–Vis spectra obtained with the addition of different OPE aliquots (from 50 to 200 μL) to a fixed quantity of $AgNO_3$ in alkaline pH condition. The spectra show a distinctive SPR band between 400 and 500 nm, typical for spherical AgNPs, varying in wavelength, width and intensity depending on the quantity of OPE extract employed. In this case, the highest, most intense, and narrowest SPR band is obtained by using 20 μL of water OPE extract in a total volume of 10 mL in ultra-pure water; these conditions were optimal to obtain a regular distribution of nanoparticles that are stabilized by the capping effect of the OPE extract, without the formation of AgNPs aggregates.

Specifically, with the increase of the OPE amount up to 20 μL, the SPR band increases while, adding higher amounts, AgNPs@OPE shows

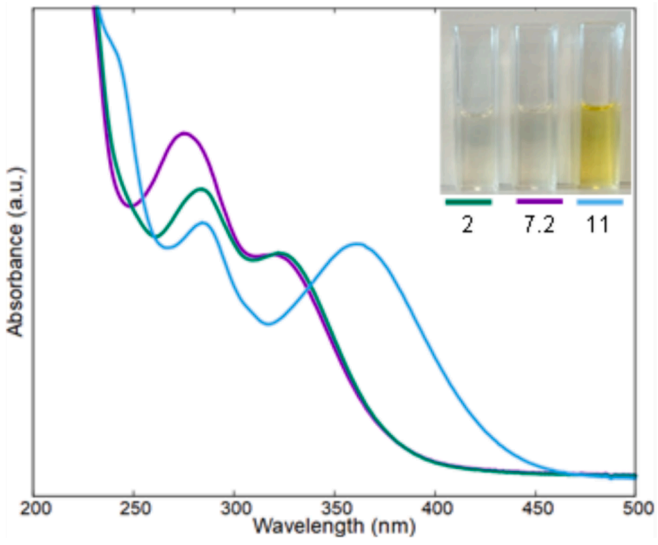

Fig 1. UV–Vis spectra of OPE extract at alkaline (sky blue), neutral (purple) and acid (green) pH.

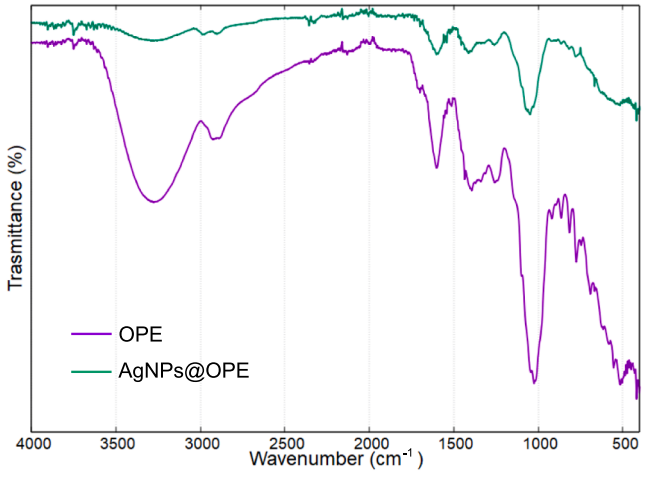

Fig. 2. FT-IR spectra of OPE extract (purple) and lyophilized AgNPs@OPE nanoparticles (green).

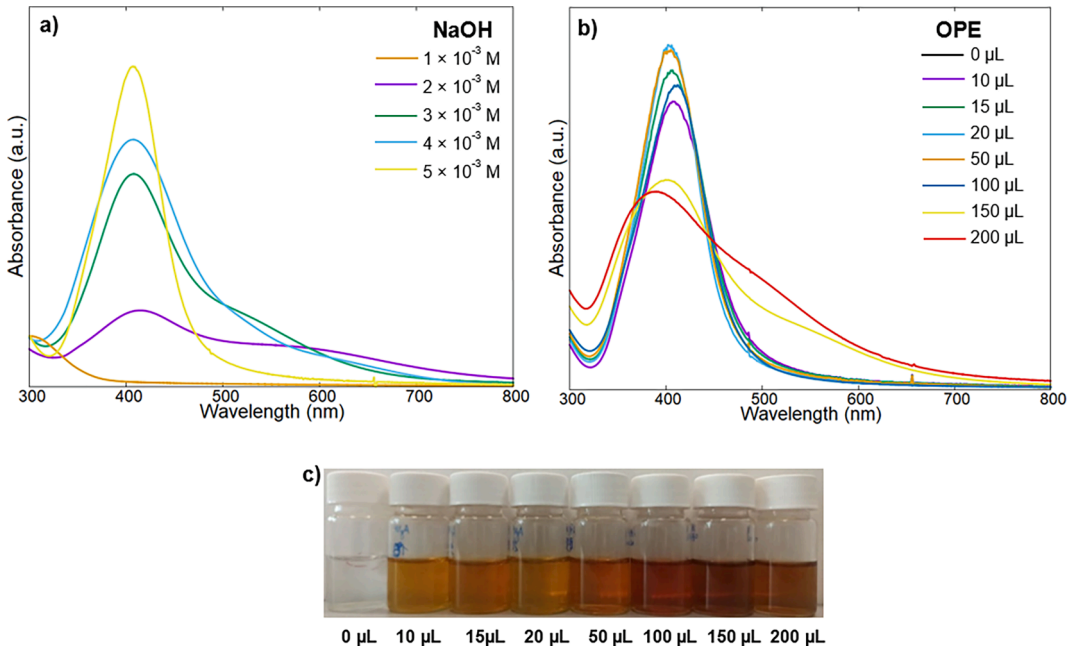

Fig. 3. UV–Vis spectra of synthesized AgNPs@OPE at a) different concentration of NaOH with 20 µL of OPE and b) different amount of OPE extract; c) samples picture of AgNPs@OPE colloidal solutions at different amount of OPE.

the typical spectra of the aggregated nanoparticles with two SPR bands, the first at lower wavelength, and the second at higher wavelength. The solution colour, from yellow to orange, reflects the spectral modifications (Fig. 3c).

As far as reaction temperature is concerned, this parameter should not go above 60 °C because, despite increasing the reaction rate, it causes a red shift and a consequent enlarge of the bands, which could be attributed to nanoparticles aggregation [30]; therefore 60 °C represents the suitable temperature to obtain stable AgNPs@OPE (Fig. S1). For these reasons, the AgNPs@OPE produced using 20 µL of OPE exctract, at 60 °C, has been used for the colorimetric assay.

3.3. Characterization of AgNPs@OPE

The FT-IR analysis (Fig. 2) of the lyophilized AgNPs@OPE shows similar profile of the OPE extract IR-spectrum, suggesting that the surface of the silver nanoparticles is bonded and functionalized by the organic water-soluble components of the orange peel extract.

The morphology of AgNPs@OPE produced by this green approach is analysed by SEM microscopy (Fig. 4a). In the Fig. 4b from the SEM image with the largest magnification, it is possible to observe the presence of quasi-spherical AgNPs@OPE; it also appears that the AgNPs@OPE are surrounded by halos, probably due to the presence of surface ligands covering the nanoparticles. The EDX spectrum in Fig. 4c confirms the presence of Ag, C and O from the OPE extract, and Na due to the NaOH used during the preparation of the nanoparticles; the presence of the Si-peak is due to the support material. The size distribution analysis of the obtained AgNPs@OPE on more than 500 nanoparticles (Fig. 4d), by using ImageJ software, shows a normal distribution and a main size at about 26.58 ± 3.21 nm; the DLS analysis of the same batch of AgNPs@OPE, reported in the Fig. 4e, show an average diameter size at around 32 nm, in accordance with the SEM measurements. In addition, the presence of negative charges on the surface of the silver nanoparticles was confirmed by the negative zeta potential value of − 42.53. ± 1.90 mV.

3.4. AgNPs@OPE as selective sensor for Cd^{2+} and Pb^{2+}

The as-prepared AgNPs@OPE are tested by UV–Vis spectroscopy by adding the same concentrations (80 µM) of different metal ions: Ca^{2+}, Cd^{2+}, Co^{2+}, Cu^{2+}, Fe^{2+}, Hg^{2+}, K^{+}, Mg^{2+}, Zn^{2+}, Na^{+}, Ni^{2+}, Mn^{2+} and Pb^{2+}. Fig. 5a shows the UV–Vis spectra of the AgNPs@OPE after the addition of each metal ion. As it can be observed, at this metal ions concentration, the typical spectra of the aggregated nanoparticles, with the formation of a new SPR band, are observed only for Cd^{2+} and Pb^{2+}, also confirmed by the different colour of the solutions, as reported in the Fig. 5c.

The pristine AgNPs@OPE, as mentioned before, show a single SPR band at 407 nm; the addition of Cd^{2+} ions produces a change in colour from yellow to red-brown (Fig. 5b), associated with a concomitant decrease and red- shift of the SPR band to 415 nm and with the formation of a new second SPR band, at 519 nm (Fig. 5a). Similarly, in presence of Pb^{2+} ions, the aggregation process lowers the intensity of the principal SPR band it is also observed a red-shift of this band to 420 nm and a visible broadening of the band together with the formation of a second SPR band centred at 545 nm. All these spectral features result in colour change from yellow to brown (Fig. 5b). The contribution in absorbance of the two SPR bands is evaluated by deconvolution process using lognormal equation, with Fityk software (Fig. S2). Specifically, during the aggregation process, the metals interact with the AgNPs@OPE, and in particular with the carboxyl/hydroxyl groups of the organic molecules contained in the OPE, bonded on the surface of the silver nanoparticles [31,32]. This interaction decreases the inter-particle distance of the nanoparticles, producing the formation of a large cluster of $(AgNPs@OPE)_n$-$(Cd^{2+})_m$ or $(AgNPs@OPE)_n$-$(Pb^{2+})_m$, promoting a chromatic variation of the colloidal suspension, the split of the principal band and the formation of the second new SPR band in the absorption profile of the AgNPs@OPE [11,33]. The colour variation can be easily detected after 15 min from the addition of the Pb^{2+} and Cd^{2+}ions. In Fig. 5c, the absorbance ratio between the principal and the secondary SPR bands, formed during the aggregation is reported: the higher change in the ratio is obtained for only Cd^{2+} and Pb^{2+}, confirming the selectivity of the AgNPs@OPE towards these two heavy metals.

3.5. Cd^{2+} and Pb^{2+} quantification by univariate approach

UV–Vis spectra of Fig. 6a show the effect of adding increasing concentrations of Pb^{2+} ions, from 2.49 to 47.62 µM to AgNPs@OPE

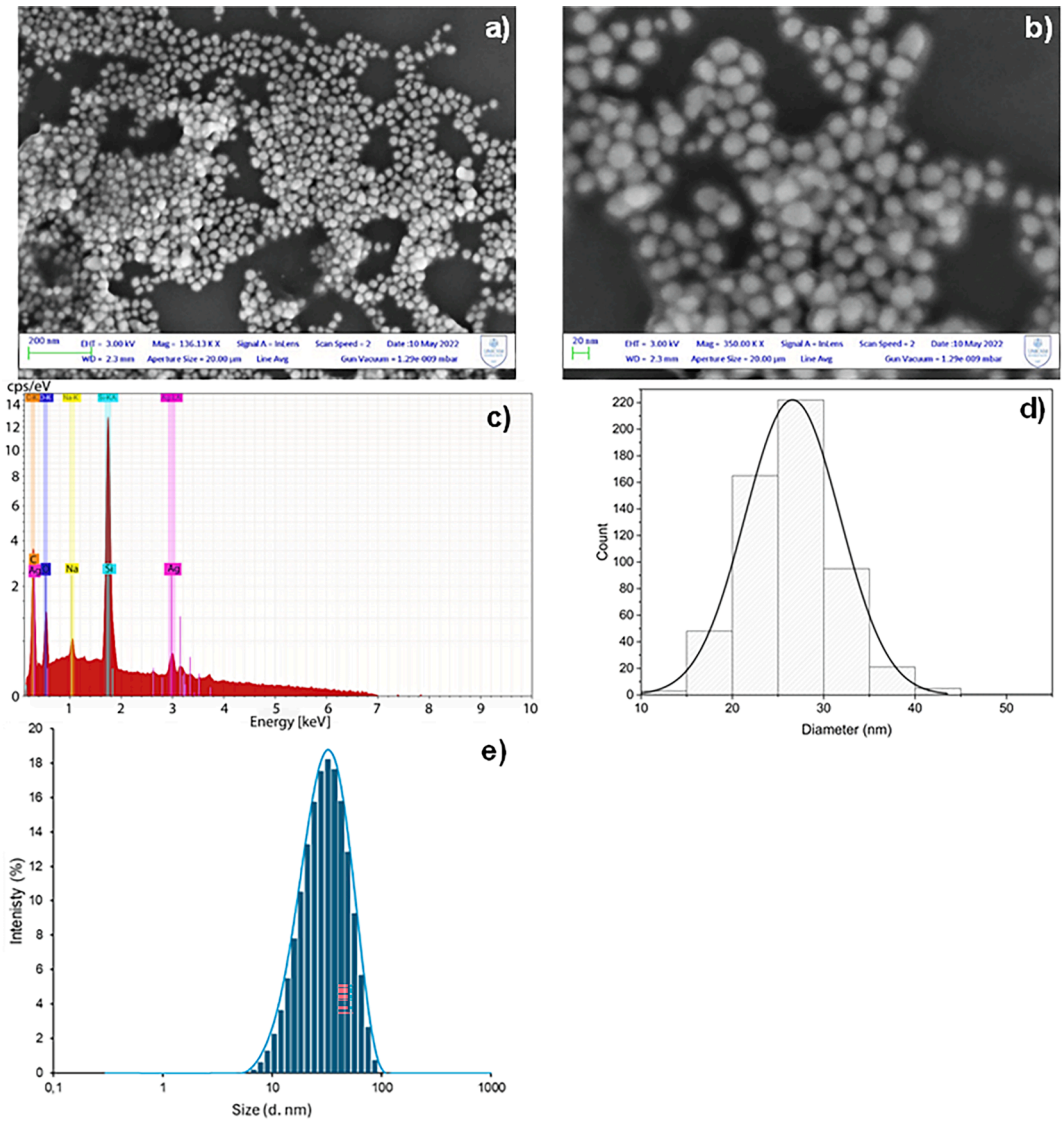

Fig. 4. A,b) sem images at different magnification, c) size distribution analysis d) edx spectrum and e) dls analysis of the agnps@ope.

colloidal solutions. From the absorbance profile it is possible to observe that, after the first addition of 2.49 μM of the Pb^{2+} ions, the main SPR band shifts to a longer wavelength (413 nm) while progressively broadens and red-shifts for each addition of Pb^{2+} ions, up to 420 nm (addition of 47.62 μM). The increasing concentration of the Pb^{2+} ions leads to a regular increase of a second broadened SPR band at 545 nm. Plotting the absorbance ratio between the two SPR bands (A_{545nm}/A_{407nm}), a sigmoidal curve, that describes the aggregation process, can be obtained (Fig. 6b). In the plot three linear region can be distinguished: the first, from 0 to 22.00 μM of Pb^{2+} ions, in which there is a gradual formation of a small lattice of AgNPs@OPE; increasing the concentration of the metal, the aggregation involves additional nanoparticles (second region) up to the third step, where the AgNPs@OPE-Pb^{2+} clusters reach the critical mass; adding higher amount of Pb^{2+} ions causes the clusters to collapse and precipitate.

For the first two linear regions of the absorbance ratio vs Pb^{2+} ions, the concentration curve is fitted with linear equations $f(x) = mx + q$; the equations with the best fitted values for the parameters m and q with 95 % confidence are reported in Fig. 6 c,d. The limits of detection (LOD) for the first and the second linear regions of the sigmoidal curve, calculated as 3 σ/m, are 5.84 and 27.13 μM, respectively. The addition of increasing amounts of Pb^{2+} ions shows a gradual change in colour of the AgNPs@OPE colloidal solutions from yellow to red/brown (Fig. 6e).

For Cd^{2+}, the obtained UV–Vis spectra upon adding increasing concentrations of Cd^{2+} ions from 2.49 to 52.01 μM to AgNPs@OPE colloidal solutions, are reported in Fig. 7a. The spectra show that after the first addition, even for Cd^{2+} there is a red-shift of the principal SPR band from 407 to 415 nm; in this case, increasing the concentration of Cd^{2+}ions, the principal SPR band decreases with the concomitant increase of the second new SPR band, centered at 519 nm. Plotting the absorbance ratio between the two SPR bands(A_{519nm}/A_{407nm}), even for Cd^{2+} ions, a sigmoidal curve can be observed (Fig. 7b). For Cd^{2+}, the linear region is identified from 9.90 to 33.82 μM Cd^{2+} and fitted with linear equations $f(x) = mx + q$; the equation with the best fitted values for the parameters m and q with 95 % confidence is reported in the Fig. 7c. The calculated limits of detection (LOD) as 3 σ/m, was 13.04 μM. Finally, as hinted above, Increasing Cd^{2+} concentration, the AgNP@OPE solution changes colour from yellow to orange (Fig. 7d) as a sign of nanoparticle aggregation.

The LOD values obtained with this green colorimetric assay, valorising a waste material are comparable with other reported AgNPs applied for the detection of Pb^{2+} and Cd^{2+} ions (Table 1); however, in the most cases, these AgNPs are chemically synthetized by specific reducing and capping agents.

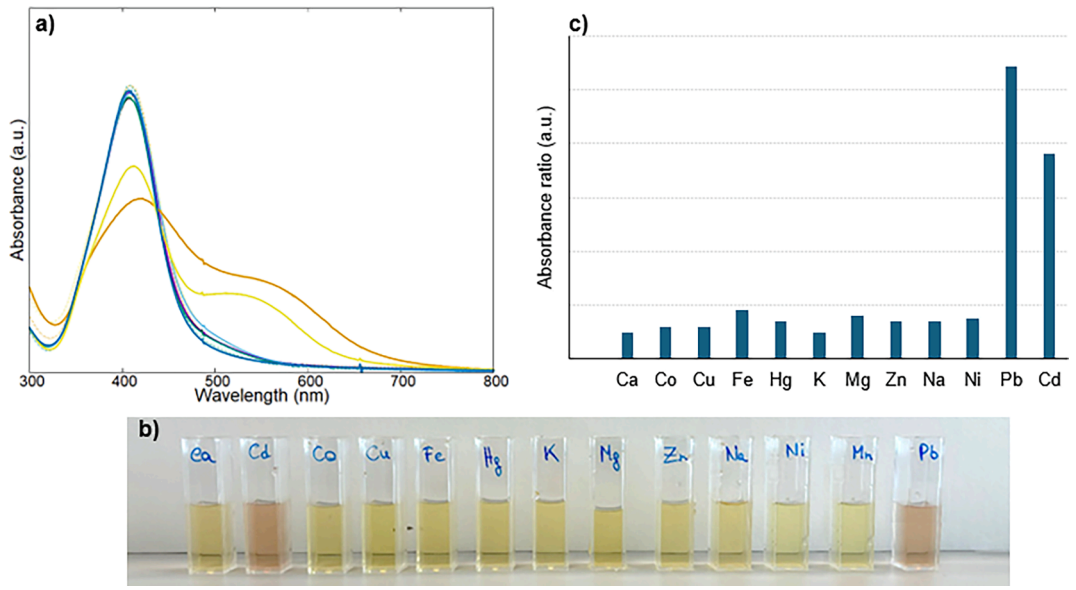

Fig. 5. A) uv–Vis spectra, b) color change solutions and c) SPR bands absorbance ratio of AgNPs@OPE after the addition of 80 μM of different metal cations in water.

3.6. Multivariate quantification of Cd^{2+} and Pb^{2+}

In the previous session, metal ion quantification has been performed calculating the absorbance ratio between the two SPR bands, identifying the different concentration ranges in which this parameter showed a linear dependence from the concentration and fitting this trend by univariate regression. To ease this procedure, multivariate calibration tools can provide an alternative approach to Cd^{2+} and Pb^{2+} quantification that relies on the information contained in the entire set of AgNPs@OPE UV–Vis spectra at different metal ion concentrations rather than on one single calculated parameter. In this case, Partial Least Square regression is applied to develop a targeted multivariate quantification model per each analyte: without going into mathematical details, this algorithm firstly reduces the dataset dimensionality by calculating new independent variables, named latent variables (LV), as linear combinations of the original ones (absorbance values at different wavelengths) that maximize the covariance with the response to be modelled, in this case, metal concentration. Then, the mathematical relationship between metal concentration and the selected latent variables is defined by Multiple Linear Regression (MLR) [26].

It must be underlined that the first LV has the maximum covariance with the response; then, the information related to LV1 is subtracted from the overall information, and LV2 is calculated in order to describe the maximum residual covariance with Y and so on. Therefore, the first LVs surely account for information actually related to the response while, moving to higher-order LV, they might account for experimental noise or other sources of variability. In order to avoid both lack of fit (too few LV) and overfitting (too many LV) issues, the proper number of LV to develop the quantification model must be identified by a suitable cross-validation or validation strategy, as already hinted above [26].

In this case, Partial Least Square regression allows the quantification of both Cd^{2+} and Pb^{2+} in the entire concentration range tested, from 2.49 to 47.62 μM without any need to reduce the concentration range and the optimal number of LV is determined by jointly evaluating RMSECV and RMSEP. RMSECV refers to the errors done by the model in predicting metal ions concentration for samples in the training set (34) during the cross-validation procedure, as described in the dedicated section; RMSEP instead depends on the prediction errors for test samples, obviously considering only the samples containing the target metal ion (4). Furthermore, the F test is applied to demonstrate the significance of the numerical differences within the two parameters, as displayed in Fig. S3 in the case of Cd^{2+} (a) and Pb^{2+}(b).

As clearly shown in the plots in Fig. S3, while RMSECV remains almost constant increasing the number of LV, RMSEP is strongly dependent on this parameter and generally presents quite high values when either few LV or high LV numbers are considered, signalling respectively lack-of-fit or overfitting issues; between these two borderline cases, robust models with satisfactory predictive performances are obtained and the optimal model is achieved considering 6 LV and 4 LV for Cd^{2+} and Pb^{2+} respectively since, in these cases, no significant difference between RMSECV and RMSEP is registered ($F_{calc} < F_{tab}$). In Fig. 8, the comparison between experimental and predicted metal ion concentrations are displayed for the optimal PLS model for Cd^{2+} (RMSECV: 4.24 μM, RMSEP: 6.59 μM) and Pb^{2+} quantification (RMSECV: 5.07 μM, RMSEP: 7.99 μM), clearly showing the model robustness and the satisfactory fitting and predictive ability.

3.7. Multivariate discrimination of Cd^{2+} and Pb^{2+}-containing AgNPs@OPE

Having already demonstrated AgNPs@OPE's selectivity towards Cd^{2+} and Pb^{2+} over other heavy metal ions and the feasibility of their application to quantify these metal ions in aqueous solution, the final step of this characterisation involves the possibility of exploiting AgNPs@OPE to distinguish between solutions containing Cd^{2+} or Pb^{2+}. Considering the evident concentration-dependent spectral changes registered for AgNPs@OPE in the presence of these metal ions and the similarity of the UV–Vis spectra in the presence of either Cd^{2+} or Pb^{2+}, the distinction between the two analytes must be performed by a multivariate approach.

Similarly to the previous case, also for this qualitative and dichotomic response, the presence of Cd^{2+} or Pb^{2+}, the entire UV–Vis spectra of the training samples is employed to build a multivariate classification model to be tested firstly by cross-validation and, secondly, by test set prediction (validation). In this case, the training samples obviously included samples containing either Cd^{2+} or Pb^{2+} at different concentrations in the range of interest (2.49—47.62 μM) since the model must be trained to distinguish between the two metal ions, regardless of their concentration.

Differently from calibration, in the case of multivariate classification algorithms, data dimensionality reduction is not strictly mandatory, but it must be applied whenever the number of variables (450) exceeds that of samples per class (34), as in this case. Therefore, the entire dataset composed by UV–Vis spectra of AgNPs@OPE added with increasing

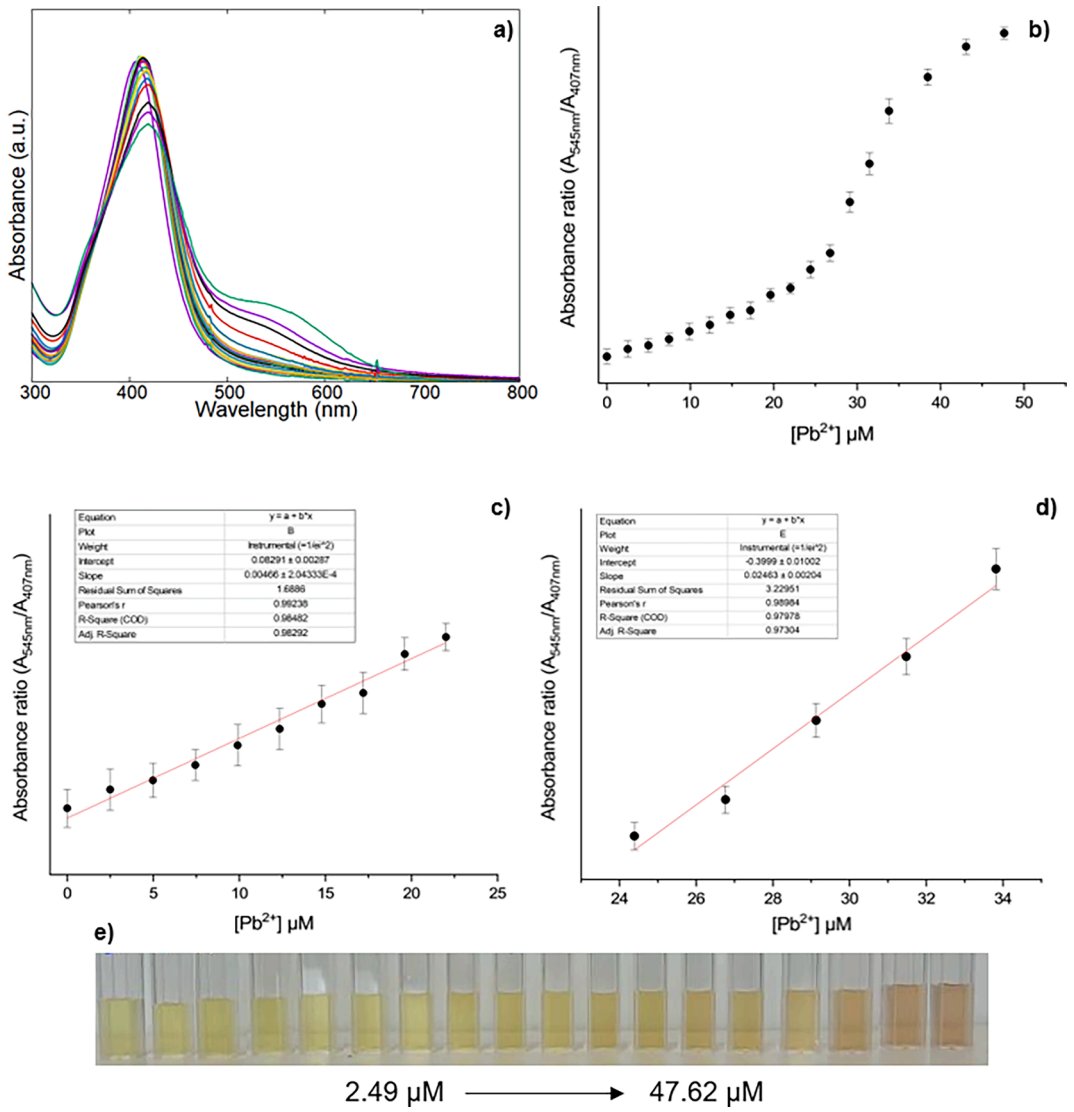

Fig. 6. A) uv–Vis spectra, b) absorbance ratio (A_{545}/A_{407}) c-d) calibration lines and e) samples image of the AgNPs@OPE at the different concentration of Pb^{2+} ions in water.

Cd^{2+} or Pb^{2+} concentration (2.49–47.62 µM) is firstly submitted to Principal Component Analysis (PCA) to reduce data dimensionality while keeping the information included in the original data. This tool allows finding new variables, named principal components (PC), as orthogonal linear combinations of the 450 original variables that maximise the explained variance; also, in this case, PC1 accounts for the highest explained variance while the percentage gradually lowers for PC2, PC3 and so on. The impact of each original variable in defining each PC's direction is expressed by the corresponding loading value. Consequently, each sample can be projected in the space defined by these new variables thus obtaining a new set of coordinates per each sample, named scores [25,26].

In this case, five principal components are computed with a decreasing percentage of explained variance (PC1:81.95 %, PC2: 7.68 %, PC3:5.28 %, PC4:2.97 % and PC5:0.97 %) and the associated loading and score values are calculated. The line plot in Fig. S4 showing the loading values vs. wavelength (nm) for the first four PCs allows us to identify which spectral region mostly impacted the separation of the samples alongside each PC; specifically, the highest impact is associated with the region presenting higher loading values, both negative or positive. An example of loadings interpretation is provided in the case of PC1: the separation alongside this component is mostly determined by signals around 415 nm, with negative loading values, and 520 nm, with positive values; the detailed interpretation of the other PCs can be performed following the same approach, but it is here omitted for brevity's sake.

Fig. 9 reports the score plots on PC1 vs. PC2 (Fig. 9a), PC2 vs. PC3 (Fig. 9b) and PC3 vs. PC4 (Fig. 9c). Analysing the samples' location in the bidimensional space defined by PC1 and PC2 (Fig. 9a), metal ions concentration exerts the main effect, with score values on PC1 increasing together with this parameter, i.e. moving samples from left to right, as shown by the arrows added to the plot; nevertheless, a tentative distinction can be observed between AgNPs@OPE containing Cd^{2+} and Pb^{2+} alongside PC2, especially at high metal concentrations.

The distinction appears much more visible in PC2 vs. PC3 score plot (Fig. 9b) with all the Cd-containing samples located in the lower part of the plot and all those containing Pb^{2+} in the upper part; also in this plot, the metal ions concentration has a visible effect, depicted by the arrows, but oppositive between the two cations. The same distinction is still partially visible in the PC3 vs. PC4 plot (Fig. 9c), where instead, no clear concentration-dependent effect can be distinguished.

In summary, PCA allows to both reduce data dimensionality and highlight the differences, even if minimal compared to those concentration-dependent, between the effect of the two metal ions on

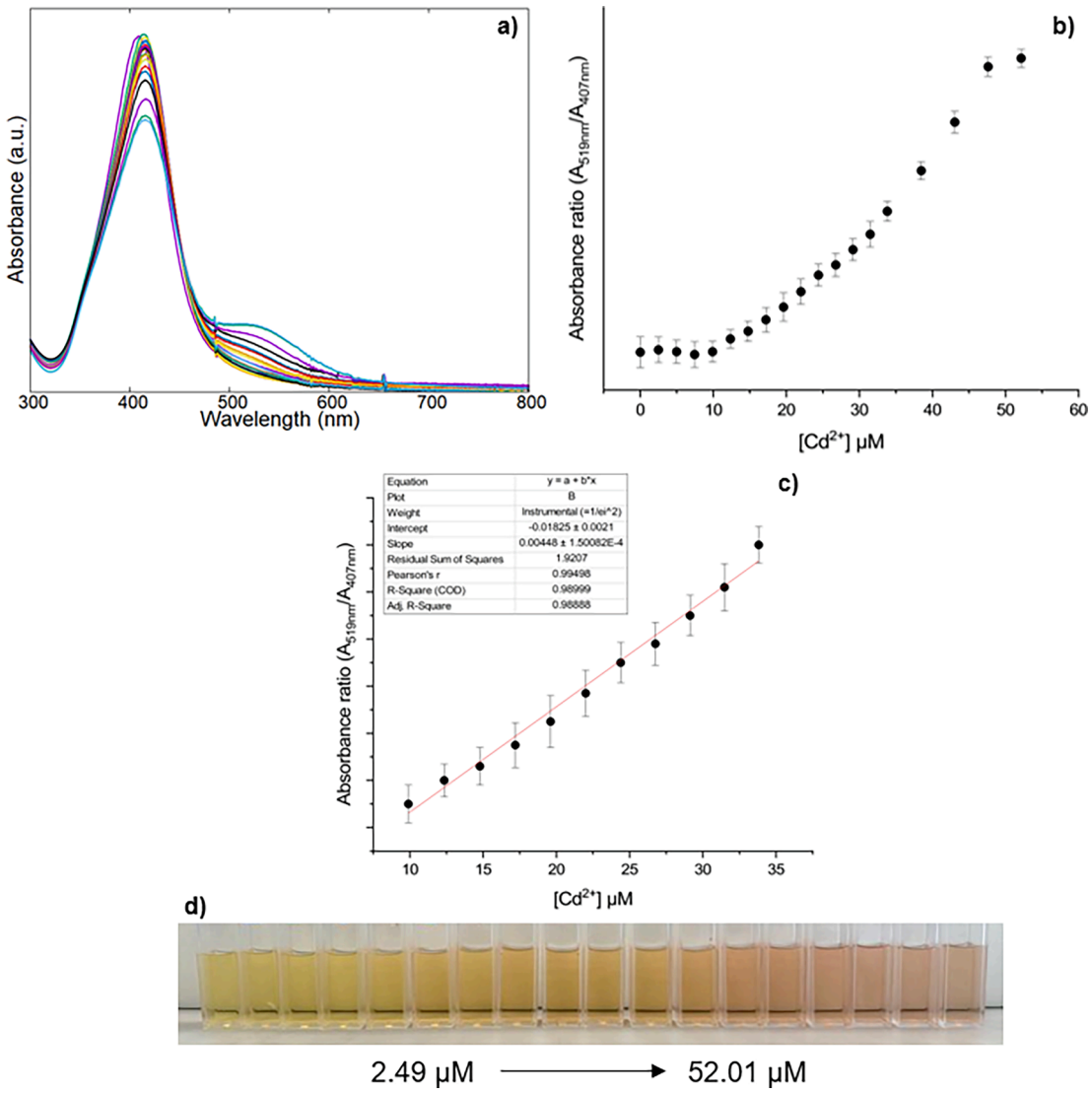

Fig. 7. A) uv–Vis spectra, b) absorbance ratio (A_{519nm}/A_{407nm}) c) calibration line and d) samples image of the AgNPs@OPE at the different concentration of Cd^{2+} ions in water.

Table 1
LOD values of the proposed method with other AgNPs-based colorimetric sensor for the determination of Pb^{2+} and Cd^{2+} in water.

Capping Agent	Detection	Linear range	LOD	
Dithizone	Pb^{2+}	2–48 µM	3 µM	[34]
Gluconate	Pb^{2+}	0.5–2.22 µM	0.203 µM	[35]
3,4-dihydroxy-L-phenylalanine	Pb^{2+}	65—125 µM	81 µM	[36]
PVA	Pb^{2+}	241 nM- 4.8 µM	0.096 µM	[37]
This work	Pb^{2+}	2.49–22 µM	5.84 µM	
5-Sulfonicanthranilic acid dithiocarbamate	Cd^{2+}	10–100 µM	5.80 µM	[38]
1-amino-2naphtol-4-sulfonic acid	Cd^{2+}	1–10 µM	0.087 µM	[39]
Chalcon carboxylic acid	Cd^{2+}	0.23–3.18 µM	0.13 µM	[40]
Grape juice	Cd^{2+}	10–150 µM	4.95 µM	[41]
Perylene dye	Cd^{2+}	–-	10 µM	[42]
This work	Cd^{2+}	9.90–33.82 µM	13.04 µM	

AgNPs@OPE UV–Vis spectra.

Finally, the score matrix (68 samples x scores on 5 PCs) is used as the input dataset to apply Linear Discriminant Analysis (LDA), a probabilistic method that calculates linear delimiters between *n* categories, two in our case, relying on probability density distributions per each class. It must be clarified that unassigned samples cannot occur in LDA since samples are always assigned to the nearest category, even if the difference is minimal and the samples are actually in proximity to the delimiter or, oppositely, they are outliers far from both the categories [25,26,43]. The developed model is first evaluated by analysing predictive performances by means of cross-validation, following the approach based on including in the cancellation group both the replicates for given concentration levels, differently chosen for the two metal ions, as already deeply discussed in the dedicated section.

CV outputs for LDA are usually presented either as “confusion matrix”, which means a matrix reporting the actual category in the rows and the predicted one in the columns, or plotting the CV Mahalanobis distance of each training sample from the centroids of all the categories, presented in form of bar plot in Fig. S5. It goes without saying that each sample is assigned by the model to the nearest class, which means the one with the smallest bar. In this case, all the samples are correctly assigned apart from one Pb-containing sample that is wrongly assigned

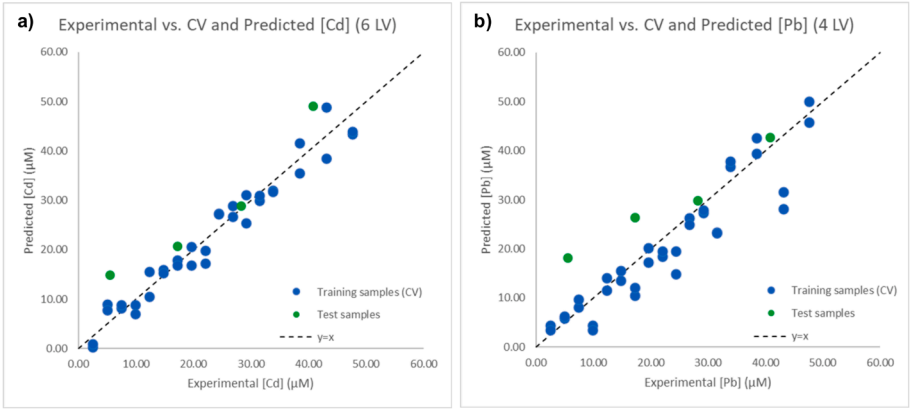

Fig. 8. Comparison between experimental and predicted metal ion concentration for training (blue) and test (green) samples in the case of Cd^{2+} (a) and Pb^{2+} quantification (b). It must be recalled that training samples prediction refers to the cross-validation procedure.

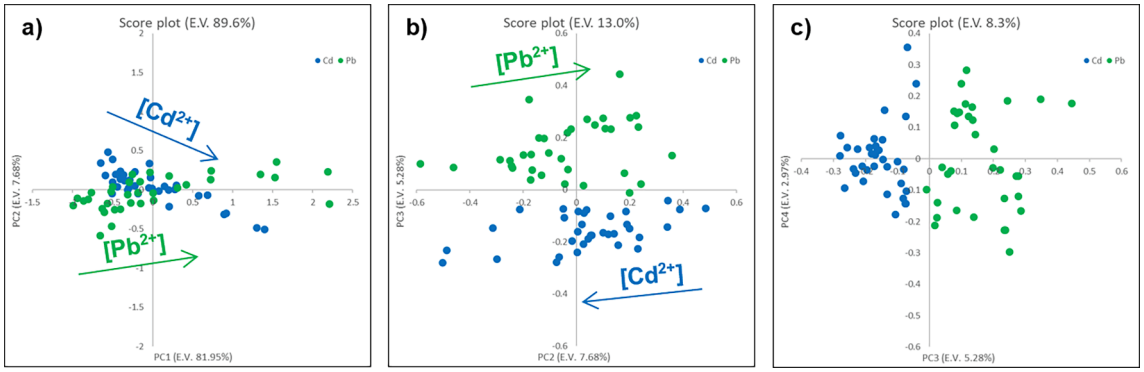

Fig. 9. Score plots on PC1 vs PC2 (a), PC2 vs PC3 (b) and PC3 vs PC4 (c) for the PCA model built on the training samples UV–Vis spectra registered for AgNPs@OPE in the presence of Cd^{2+} or Pb^{2+}.

to the Cd category, even if the two distances are quite similar. The overall percentage of correct prediction is 98.5 % for training samples in CV [25,26,43].

Once developed and firstly evaluated, the classification model is tested on independent samples containing either Cd^{2+} or Pb^{2+}, in concentrations included in the range used for building the model (5.47, 17.20, 28.18 and 40.76 μM for each metal ion), or both the metal ions, selecting three values of cumulative metal ions concentrations (5.47, 28.18 and 40.76 μM) and three Cd/Pb ratios (9:1, 1:1 and 1:9). Clearly, test samples must be submitted to the same data treatment applied for the training ones: they must be firstly projected in the PCA model, multiplying the already computed loading values for the centred original variables and obtaining the corresponding set of score values per each test sample, that are secondly submitted to LDA model to predict the category.

Table 2 and Fig. 10 summarise the results obtained for test set prediction by LDA applied on Principal Components, reporting both the predicted category per each test sample (Table 2) and the Mahalanobis distance bar plot (Fig. 10). Test samples containing only Cd^{2+}, from 5.49 to 40.76 μM, are correctly assigned to the Cd category, while the presence of Pb^{2+} is correctly identified only at higher concentrations (28.18 and 40.76 μM). Analysing Fig. 10, we can observe that samples at low Pb^{2+} concentration present a quite similar Mahalanobis distance from the two centroids, thus suggesting that they are located in proximity to the delimiter and, therefore, the category assignment may vary just due to experimental variability. As for mixed samples, when the cumulative metal ion concentration is 5.47 μM, the presence of Pb^{2+} is never recognised, as it can be expected from the results on samples containing only this metal ion. Opposite, when the cumulative metal ion concentration is higher, in samples with a Cd/Pb ratio of 1:1, the distance between the two centroids is not so different, even if assigned to the Cd class, while those with a 1:9 ratio are correctly assigned to the Pb category, even in the presence of Cd^{2+}. These interesting results allow to demonstrate the robustness and effectiveness of the developed model in distinguishing between Cd and Pb-containing AgNPs@OPE.

Table 2
Predicted category for each sample in the test set.

Test sample	$[Cd^{2+}]$ (μM)	$[Pb^{2+}]$ (μM)	Class
Cd 5.47 μM	5.47	0.0	Cd
Cd 17.20 μM	17.20	0.0	Cd
Cd 28.18 μM	28.18	0.0	Cd
Cd 40.76 μM	40.76	0.0	Cd
Pb 5.47 μM	0.0	5.47	Cd
Pb 17.20 μM	0.0	17.20	Cd
Pb 28.18 μM	0.0	28.18	Pb
Pb 40.76 μM	0.0	40.76	Pb
Cd-Pb (5.47 μM) 9:1	4.92	0.55	Cd
Cd-Pb (5.47 μM) 1:1	2.74	2.74	Cd
Cd-Pb (5.47 μM) 1:9	0.55	4.92	Cd
Cd-Pb (28.18 μM) 9:1	25.36	2.82	Cd
Cd-Pb (28.18 μM) 1:1	14.09	14.09	Cd
Cd-Pb (28.18 μM) 1:9	2.82	25.36	Pb
Cd-Pb (40.76 μM) 9:1	36.69	4.08	Cd
Cd-Pb (40.76 μM) 1:1	20.38	20.38	Cd
Cd-Pb (40.76 μM) 1:9	4.08	36.69	Pb

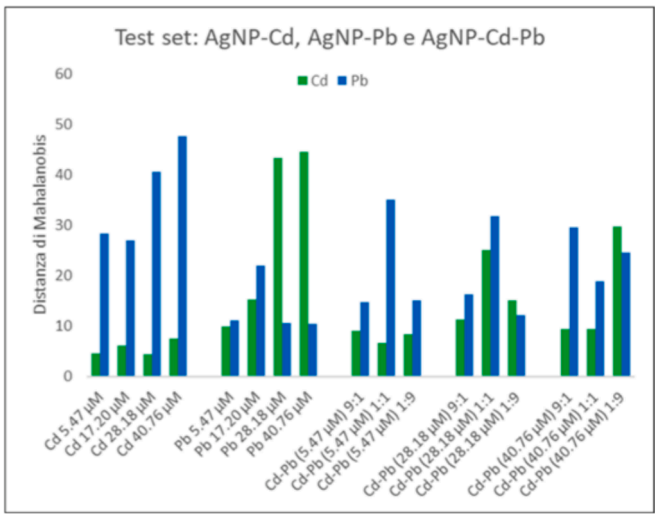

Fig. 10. Mahalanobis distance from the centroids of Cd (green) and Pb (blue) categories for each sample in the test set.

3.8. AgNPs@OPE sensor application for Cd^{2+} and Pb^{2+} quantification and discrimination in fortified real samples

Eventually, AgNPs@OPE ability to quantify and distinguish between Cd^{2+} and Pb^{2+} is tested also in fortified samples of tap water in order to confirm the robustness of both sensing mechanism and data treatment approach to matrix-related effect. The tap water used is firstly characterized by ICP-MS and IC analysis to quantify the main metal ions, and the possible interferents, the results are reported in Table S3. The tap water is then fortified with Cd^{2+} or Pb^{2+} or both the analytes in the respective concentrations reported in the Table S1. All the fortified tap water samples are characterized by UV–Vis spectroscopy (Figure S6) and those containing only one analyte are employed to test the robustness of the respective PLS model while all the samples, containing both one or two analytes, are used to validate the LDA model run on PCA outputs.

As for the evaluation of PLS models robustness, the comparisons between experimental and predicted metal ions concentration, both for the training set (CV predicted) and the two test sets, are reported in Fig. 11a and b: at a glance, the distribution around y = x line for fortified tap water samples (red circles) do not significantly differ from that for training (blue) and test (green) samples previously presented. To confirm this preliminary assumption, F test is employed to confirm that the difference between RMSECV or RMSEP for synthetic samples and RMSEP for fortified tap water samples is not significant: for both the metal ions, RMSEP in fortified tap water is equal to both RMSECV and RMSEP for synthetic samples, being F_{calc} always lower than F_{tab}, as reported in Table 3.

Lastly, fortified tap water samples, containing either one or both the metal ions, are submitted to the discrimination model to test also its robustness towards matrix-related effects: as already discussed for the synthetic test samples, also these test points are previously projected into the PCA model and the so-obtained score values are submitted to LDA to distinguish between Cd and Pb-containing AgNPs@OPE. As shown in Fig. 11c, in presence of only one metal ion, either Cd^{2+} or Pb^{2+}, LDA model perfectly recognises which metal ion has been added to AgNPs@OPE but also, when both metal ions are present, the predominant amount of both Cd^{2+} and Pb^{2+} in 6:1 or 1:6 samples is correctly identified. Only in samples containing almost equimolar mixtures of the analytes (2:1 and 1:2), the classification results are less satisfactory.

Nevertheless, the results obtained for both Cd^{2+} and Pb^{2+} quantification and discrimination in fortified tap water samples lead to promising results for the application of AgNPs@OPE as selective sensors in real samples.

4. Conclusions

Silver nanoparticles (AgNPs@OPE) are prepared by an environmentally friendly procedure using water orange peel extract as a reducing, capping and stabilizing agent under alkaline conditions.

Comparing the optimized AgNPs@OPE with other reported AgNPs, produced by orange/citrus peel extract, this green procedure permits to obtain a regular distribution of the AgNPs@OPE with the absence of nanoparticles aggregates [17–20,30,44], confirmed by the narrow SPR band at 407 nm detected by UV–Vis spectroscopy, and by the SEM analysis.

The as-prepared AgNPs@OPE are tested as colorimetric sensors in aqueous solutions containing different metal ions. The colorimetric assay shows selectivity towards Cd^{2} and Pb^{2+}; in presence of the two target cations the UV–Vis spectra display the typical behaviour of the aggregation process, with the split of the principal SPR band at 407 nm, and the formation of a new second band at a higher wavelength at 519 nm and 545 nm, for Cd^{2+} and Pb^{2+}, respectively. The first approach is

Table 3
Cross-Validation and Prediction statistics for PLS models for Cd^{2+} and Pb^{2+} quantification.

Test sample	Cd^{2+}	Pb^{2+}
RMSEP in tap water	3.75	6.11
RMSECV	4.24	5.07
F_{calc}	1.28	1.45
F_{tab}	8.61	2,89
RMSEP in synthetic samples	6.59	7.99
F_{calc}	3.08	1.71
F_{tab}	9.12	9.12

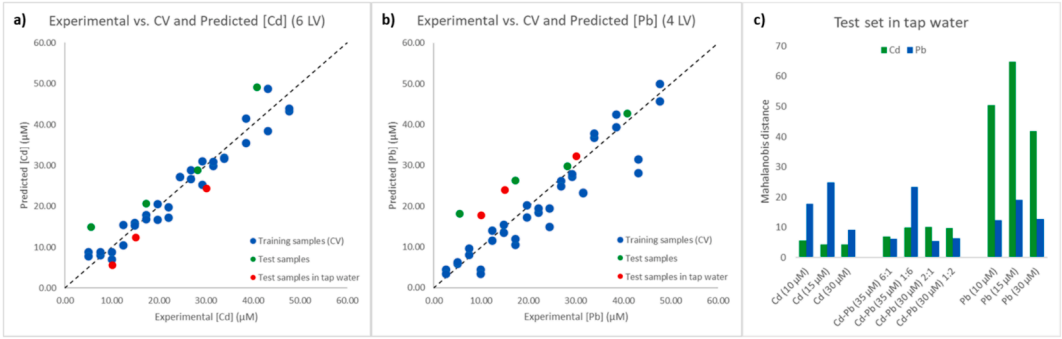

Fig. 11. Comparison between experimental and predicted metal ion concentration for training (blue) and test synthetic samples (green) or fortified tap water ones (red) in the case of Cd^{2+} (a) and Pb^{2+} quantification (b) and Mahalanobis distance from the centroids of Cd (green) and Pb (blue) categories for each sample in the test fortified tap water samples (c). It must be recalled that training samples prediction refers to the cross-validation procedure.

the metal ion quantification in the linearity range by univariate regression monitoring the linear dependence of the absorbance ratio between the two SPR bands from the concentration. The LOD calculated from the linear univariate regression is 5.84 μM and 10.34 μM for Pb^{2+} and Cd^{2+}, respectively. Then, PLS is applied to quantify the two metal ions in the entire concentration range tested, relying on the information contained in the entire UV–Vis spectra, achieving an RMSEP of 6.59 μM and 7.99 μM for Cd^{2+} and Pb^{2+}, respectively. In addition, UV–Vis spectra registered both in the presence of Cd^{2+} and Pb^{2+} are employed to compute a classification model able to distinguish which one of the two target cations is added to AgNPs@OPE. This goal is achieved by first submitting the dataset to PCA and, secondly, using PCA scores as input data for LDA. The so-built model demonstrates satisfactory predictive performances in unknown samples containing both one and two target metal ions. Finally, the AgNPs@OPE ability to quantify and distinguish between Cd^{2+} and Pb^{2+} is tested also in fortified samples of tap water in order to confirm the robustness of both sensing mechanism and data treatment approach to matrix-related effect; the results obtained for both the cations quantification and discrimination lead to promising results for the application of AgNPs@OPE as selective sensors in real samples.

CRediT authorship contribution statement

Marco Zannotti: Writing – review & editing, Software, Methodology, Data curation, Conceptualization. **Sara Piras:** Writing – original draft, Formal analysis, Data curation. **Lisa Rita Magnaghi:** Writing – original draft, Software, Methodology, Data curation, Conceptualization. **Raffaela Biesuz:** Writing – review & editing, Supervision. **Rita Giovannetti:** Writing – review & editing, Supervision, Project administration, Funding acquisition, Conceptualization.

Declaration of competing interest

The authors declare that they have no known competing financial interests or personal relationships that could have appeared to influence the work reported in this paper.

Data availability

Data will be made available on request.

Acknowledgements

This work was financially supported by MUR (Italy) and, specifically, by the Programma Operativo Nazionale Ricerca e Innovazione 2014-2020 (PON, CCI 2014IT16M2OP005, ESF REACT-EU resources, Action IV.4) to deliver research on “Material and methods for environmental applications”.

Appendix A. Supplementary data

Supplementary data to this article can be found online at https://doi.org/10.1016/j.saa.2024.124881.

References

[1] J. Briffa, E. Sinagra, R. Blundell, Heavy metal pollution in the environment and their toxicological effects on humans, Heliyon 6 (2020) e04691, https://doi.org/10.1016/j.heliyon.2020.e04691.
[2] C. Zamora-Ledezma, D. Negrete-Bolagay, F. Figueroa, E. Zamora-Ledezma, M. Ni, F. Alexis, V.H. Guerrero, Heavy metal water pollution: A fresh look about hazards, novel and conventional remediation methods, Environ. Technol. Inno. 22 (2021) 101504, https://doi.org/10.1016/j.eti.2021.101504.
[3] A.A. Markeb, J. Moral-Vico, A. Sánchez, X. Font, Optimization of lead (II) removal from water and wastewater using a novel magnetic nanocomposite of aminopropyl triethoxysilane coated with carboxymethyl cellulose cross-linked with chitosan nanoparticles, Arab. J. Chem. 16 (2023) 105022, https://doi.org/10.1016/j.arabjc.2023.105022.
[4] G. Genchi, M.S. Sinicropi, G. Lauria, A. Carocci, A. Catalano, The Effects of Cadmium Toxicity, Int. J. Environ. Res. Public Health 17 (2020) 3782, https://doi.org/10.3390/ijerph17113782.
[5] G. Magdy E. Aboelkassim S.M. Abd Elhaleem F. Belal A comprehensive review on silver nanoparticles: Synthesis approaches, characterization techniques, and recent pharmaceutical, environmental, and antimicrobial applications Microchem. J. 196 (2024) 109615 10.1016/j.microc.2023.109615.
[6] J. Khodaveisi, A.M.H. Shabani, S. Dadfarnia, M.R. Moghadam, M.R. Hormozi-Nezhad, Simultaneous Determination of Protocatechuic Aldehyde and Protocatechuic Acid Using the Localized Surface Plasmon Resonance Peak of Silver Nanoparticles and Chemometric Methods, Quim Nova 38 (2015) 896–901, https://doi.org/10.5935/0100-4042.20150084.
[7] G. Vinci, M. Rapa, Noble Metal Nanoparticles Applications: Recent Trends in Food Control, Bioengineering 6 (2019) 10, https://doi.org/10.3390/bioengineering6010010.
[8] F.Y. Alzoubi, A.A. Ahmad, I.A. Aljarrah, A.B. Migdadi, Q.M. Al-Bataineh, Localize surface plasmon resonance of silver nanoparticles using Mie theory, J. Mater. Sci. : mater. Elecetron. 34 (2023) 2128, https://doi.org/10.1007/s10854-023-11304-x.
[9] J. Helmlinger, C. Sengstock, C. Gross-Heitfeld, C. Mayer, T.A. Schildhauer, M. Köller, M. Epple, Silver nanoparticles with different size and shape: equal cytotoxicity, but different antibacterial effects, RSC Adv. 6 (2016) 18490–18501, https://doi.org/10.1039/c5ra27836h.
[10] M. Zannotti, V. Vicomandi, A. Rossi, M. Minicucci, S. Ferraro, L. Petetta, R. Giovannetti, Tuning of hydrogen peroxide etching during the synthesis of silver nanoparticles. An application of triangular nanoplates as plasmon sensors for Hg in aqueous solution, J. Mol. Liq. 309 (2020) 113238, https://doi.org/10.1016/j.molliq.2020.113238.
[11] A. Rossi, M. Zannotti, M. Cuccioloni, M. Minicucci, L. Petetta, M. Angeletti, R. Giovannetti, Silver Nanoparticle-Based Sensor for the Selective Detection of Nickel Ions, Nanomaterials 11 (2021) 1733, https://doi.org/10.3390/nano11071733.
[12] G. Alberti, C. Zanoni, L.R. Magnaghi, R. Biesuz, Gold and Silver Nanoparticle-Based Colorimetric Sensors: New Trends and Applications, Chemosensors 9 (2021) 305, https://doi.org/10.3390/chemosensors9110305.
[13] R.R. Vidyasagar, S.K. Patel, M. Singh, Singh, Green synthesis of silver nanoparticles: methods, biological applications, delivery and toxicity, Mater. Adv. 4 (2023) 1831–1849, https://doi.org/10.1039/d2ma01105k.
[14] A. Zuhrotun, D.J. Oktaviani, A.N. Hasanah, Biosynthesis of Gold and Silver Nanoparticles Using Phytochemical Compounds, Molecules 28 (2023) 3240, https://doi.org/10.3390/molecules28073240.
[15] P. Sathishkumar, F.L. Gu, Q.Q. Zhan, T. Palvannan, A.R.M. Yusoff, Flavonoids mediated 'Green' nanomaterials: A novel nanomedicine system to treat various diseases - Current trends and future perspective, Mater. Lett. 210 (2018) 26–30, https://doi.org/10.1016/j.matlet.2017.08.078.
[16] M.G. Peña-Juarez, P.C. Mayorga-Colunga, C.A. Rivera-Hernandez, E.J. Gutierrez-Castañeda, J. Navarrete-Damián, E. Pérez, J.A. Gonzalez-Calderon, Feasibility of quercetin dietary supplement as reducing and stabilizing agent: Green route of silver nanoparticles using a bioactive flavonoid, MRS Commun. 11 (2021) 498–503, https://doi.org/10.1557/s43579-021-00063-7.
[17] J. Yadav, P. Chauhan, Green synthesis of silver nanoparticles using Citrus X sinensis (Orange) fruit extract and assessment of their catalytic reduction, Mater Today Proc. 62 (2022) 6177–6181, https://doi.org/10.1016/j.matpr.2022.05.041.
[18] A. Bratovcic, A. Dautovic, Green Synthesis of Silver Nanoparticles Using Aqueous Orange and Lemon Peel Extract and Evaluation of Their Antimicrobial Properties, Advances in Nanoparticles 13 (2024) 11–28, https://doi.org/10.4236/anp.2024.132002.
[19] Y.S. Mostafa, S.A. Alamri, S.A. Alrumman, M. Hashem, Z.A. Baka, Green Synthesis of Silver Nanoparticles Using Pomegranate and Orange Peel Extracts and Their Antifungal Activity against, the Causal Agent of Early Blight Disease of Tomato, Plants 10 (2021) 2363, https://doi.org/10.3390/plants10112363.
[20] E.A. Terenteva, V.V. Apyari, S.G. Dmitrienko, Y.A. Zolotov, Formation of plasmonic silver nanoparticles by flavonoid reduction: A comparative study and application for determination of these substances, Spectrochim. Acta A 151 (2015) 89–95, https://doi.org/10.1016/j.saa.2015.06.049.
[21] L.M. Carrascal, I. Galván, O. Gordo, Partial least squares regression as an alternative to current regression methods used in ecology, Oikos 118 (2009) 681–690, https://doi.org/10.1111/j.1600-0706.2008.16881.x.
[22] H. Abdi, Partial least squares regression and projection on latent structure regression (PLS Regression), WIREs Comput. Stat. 2 (2010) 97–106, https://doi.org/10.1002/wics.51.
[23] I.S. Helland, Some theoretical aspects of partial least squares regression, Chemometr Intell Lab 58 (2001) 97–107, https://doi.org/10.1016/S0169-7439(01)00154-X.
[24] R. Bro, A.K. Smilde, Principal component analysis, Anal. Methods 6 (2014) 2812–2831, https://doi.org/10.1039/c3ay41907j.
[25] P. Oliveri, C. Malegori, M. Casale, Chemometrics and Statistics | Multivariate Classification Techniques, in: P. Worsfold, C. Poole, A. Townshend, M. Miró (Eds.), Encyclopedia of Analytical Science (third Edition), Academic Press, Oxford, 2019, pp. 481–486, https://doi.org/10.1016/B978-0-12-409547-2.14239-8.
[26] P. Oliveri, M. Chiara Casolino, M. Forina, Chapter 2 - Chemometric Brains for Artificial Tongues, in: S.L. Taylor (Ed.) Advances in Food and Nutrition Research, Academic Press 2010, pp. 57-117. 10.1016/B978-0-12-374468-5.00002-7.
[27] L. Riccardo, P. Gianmarco, M. Camillo, CAT (Chemometric Agile Tool), freely downloadable from http://gruppochemiometria.it/index.php/software.

[28] N. Jayaprakash, R. Suresh, S. Rajalakshmi, S. Raja, E. Sundaravadivel, M. Gayathri, M. Sridharan, One-step synthesis, characterisation, photocatalytic and bio-medical applications of ZnO nanoplates, Mater. Technol. 35 (2020) 112-124 10.1080/10667857.2019.1659533.
[29] M. Krysa, M. Szymanska-Chargot, A. Zdunek, FT-IR and FT-Raman fingerprints of flavonoids - A review, Food. Chem. 393 (2022) 133430, https://doi.org/10.1016/j.foodchem.2022.133430.
[30] P. Saha, M. Mahiuddin, A.B.M.N. Islam, B. Ochiai, Biogenic Synthesis and Catalytic Efficacy of Silver Nanoparticles Based on Peel Extracts of Citrus macroptera Fruit, ACS Omega 6 (2021) 18260–18268, https://doi.org/10.1021/acsomega.1c02149.
[31] G.W. Zhong, J.X. Liu, X.Y. Liu, A Fast Colourimetric Assay for Lead Detection Using Label-Free Gold Nanoparticles (AuNPs), Micromachines 6 (2015) 462–472, https://doi.org/10.3390/mi6040462.
[32] X. Mao, Z.P. Li, Z.Y. Tang, One pot synthesis of monodispersed L-glutathione stabilized gold nanoparticles for the detection of Pb ions, Front, Mater. Sci. 5 (2011) 322–328, https://doi.org/10.1007/s11706-011-0118-4.
[33] A. Rossi, M. Cuccioloni, L.R. Magnaghi, R. Biesuz, M. Zannotti, L. Petetta, M. Angeletti, R. Giovannetti, Optimizing the heavy metal ion sensing properties of functionalized silver nanoparticles: the role of surface coating density, Chemosensors 10 (2022) 483, https://doi.org/10.3390/chemosensors10110483.
[34] R. Roto, B. Mellisani, A. Kuncaka, M. Mudasir, A. Suratman, Colorimetric Sensing of Pb Ion by Using Ag Nanoparticles in the Presence of Dithizone, Chemosensors 7 (2019) 28, https://doi.org/10.3390/chemosensors7030028.
[35] R. Choudhury, T.K. Misra, Gluconate stabilized silver nanoparticles as a colorimetric sensor for Pb, Colloid Surface A 545 (2018) 179–187, https://doi.org/10.1016/j.colsurfa.2018.02.051.
[36] J.Y. Cheon, W.H. Park, Green Synthesis of silver nanoparticles stabilized with Mussel-Inspired protein and colorimetric sensing of Lead(II) and Copper(II) Ions, Int J Mol Sci 17 (2016) 2006, https://doi.org/10.3390/ijms17122006.
[37] K. Shrivas, B. Sahu, M.K. Deb, S.S. Thakur, S. Sahu, R. Kurrey, T. Kant, T.K. Patle, R. Jangde, Colorimetric and paper-based detection of lead using PVA capped silver nanoparticles: Experimental and theoretical approach, Microchem J 150 (2019) 104156, https://doi.org/10.1016/j.microc.2019.104156.
[38] V.N. Mehta, J.V. Rohit, S.K. Kailasa, Functionalization of silver nanoparticles with 5-sulfoanthranilic acid dithiocarbamate for selective colorimetric detection of Mn and Cd ions, New J Chem 40 (2016) 4566–4574, https://doi.org/10.1039/c5nj03454j.
[39] P.C. Huang, B.W. Liu, W.W. Jin, F.Y. Wu, Y.Q. Wan, Colorimetric detection of Cd using 1-amino-2-naphthol-4-sulfonic acid functionalized silver nanoparticles, J Nanopart Res 18 (2016) 327, https://doi.org/10.1007/s11051-016-3630-8.
[40] Y.J. Dong, L.L. Ding, X. Jin, N.N. Zhu, Silver nanoparticles capped with chalcon carboxylic acid as a probe for colorimetric determination of cadmium(II), Microchim Acta 184 (2017) 3357–3362, https://doi.org/10.1007/s00604-017-2358-1.
[41] S. Jabariyan, M.A. Zanjanchi, Colorimetric detection of cadmium ions using modified silver nanoparticles, Appl Phys a-Mater 125 (2019) 872, https://doi.org/10.1007/s00339-019-3167-7.
[42] Y.M. Guo, Y. Zhang, H.W. Shao, Z. Wang, X.F. Wang, X.Y. Jiang, Label-Free colorimetric detection of cadmium ions in rice samples using gold nanoparticles, Anal Chem 86 (2014) 8530–8534, https://doi.org/10.1021/ac502461r.
[43] P. Oliveri, C. Malegori, E. Mustorgi, M. Casale, Qualitative pattern recognition in chemistry: Theoretical background and practical guidelines, Microchem. J. 162 (2021) 105725, https://doi.org/10.1016/j.microc.2020.105725.
[44] I. Ghiuță, Silver Nanoparticles Synthesized by Orange Peel Extract Recent J. 71 (2023) 269-273 10.31926/RECENT.2023.71.269 269.